

ROBOTIC AND MULTIAXIAL TESTING FOR THE CONSTITUTIVE CHARACTERIZATION OF COMPOSITES

John Michopoulos, Naval Research Laboratory, Code 6394, Washington, DC, USA  
 Athanasios Iliopoulos, George Mason University, resident at NRL, Washington, DC, USA  
 John Hermanson, Forest Products Laboratory, Madison, Wisconsin, USA

ABSTRACT

As wind energy production drives the manufacturing of wind turbine blades, the utilization of glass and carbon fiber composites as a material of choice continuously increases. Consequently, the needs for accurate structural design and material qualification and certification as well as the needs for aging predictions further underline the need for accurate constitutive characterization of composites. In the present paper we describe an outline of a recently developed methodology that utilizes multi-axial robotically controlled testing combined with design optimization for the automated constitutive characterization of composite materials for both the linear and non-linear regimes. Our approach is based on the generation of experimental data originating from custom-developed mechatronic material testing systems that can expose specimens to multidimensional loading paths and can automate the acquisition of data representing the excitation and response behavior of the specimens involved. Material characterization is achieved by minimizing the difference between experimentally measured and analytically computed system responses as described by strain fields and surface strain energy densities. Small and finite strain formulations based on strain energy density decompositions are developed and utilized for determining the constitutive behavior of composite materials. Examples based on actual data demonstrate the successful application of design optimization for constitutive characterization. Validation experiments and their comparisons to theoretical predictions demonstrate the power of this approach.

INTRODUCTION

The process of designing any structure interacting with a fluid, such that of a wind turbine blade in an air-stream, requires the ability to model the interaction for the two continua in the applicable multiphysics context. The aero-structural behavior of such a system can be described by a system of partial differential equations (PDEs)<sup>1</sup>.

In fact, if we let  $\tilde{\chi}_t$  denote a continuous mapping from a reference fluid configuration  $\Omega_F(t)|_{t=0} \subset \mathbb{R}^3$  to a current fluid configuration  $\Omega_F(t) \subset \mathbb{R}^3$  such that

$$\tilde{\chi}_t : \Omega_F(t)|_{t=0} \longrightarrow \Omega_F(t), x(\xi, t) = \tilde{\chi}_t(\xi), \quad (1)$$

where  $t \in [0, \infty]$  denotes time,  $x(\xi, t)$  denotes the time-dependent position vector of a fluid point,  $\xi$  its position in reference configuration, and  $J = |\partial x / \partial \xi|$  denotes the Jacobian determinant of the deformation gradient, then the relevant PDEs take the form,

$$\frac{\partial(Jw)}{\partial t} \Big|_{\xi} + J\nabla_x \cdot (F(w) - \frac{\partial x}{\partial t} \Big|_{\xi} w) = J\nabla_x \cdot R(w) + JS(w), \text{ in } \Omega_F \quad (2a)$$

$$\rho_S \frac{\partial^2 u_S}{\partial t^2} - \nabla_x \tilde{\sigma}_S(\tilde{\epsilon}_S) = b, \text{ in } \Omega_S \quad (2b)$$

$$\rho_f \frac{\partial^2 x}{\partial t^2} \Big|_{\xi} - \nabla_{\xi} \tilde{\sigma}_f(x - x|_{t=0}) = 0, \text{ in } \Omega_F \quad (2c)$$

Equation (2a) represents the arbitrary Lagrangian Eulerian (ALE) form of the Navier-Stokes equations where  $w$  denotes the conservative fluid state vector,  $F$  and  $R$  denote the convective and diffusive fluxes, respectively. The quantity  $S(w)$  denotes the source term associated with a potential turbulence model. Equations (2b) and (2c) represent the equations of motion for the solid and fluid phases, respectively.

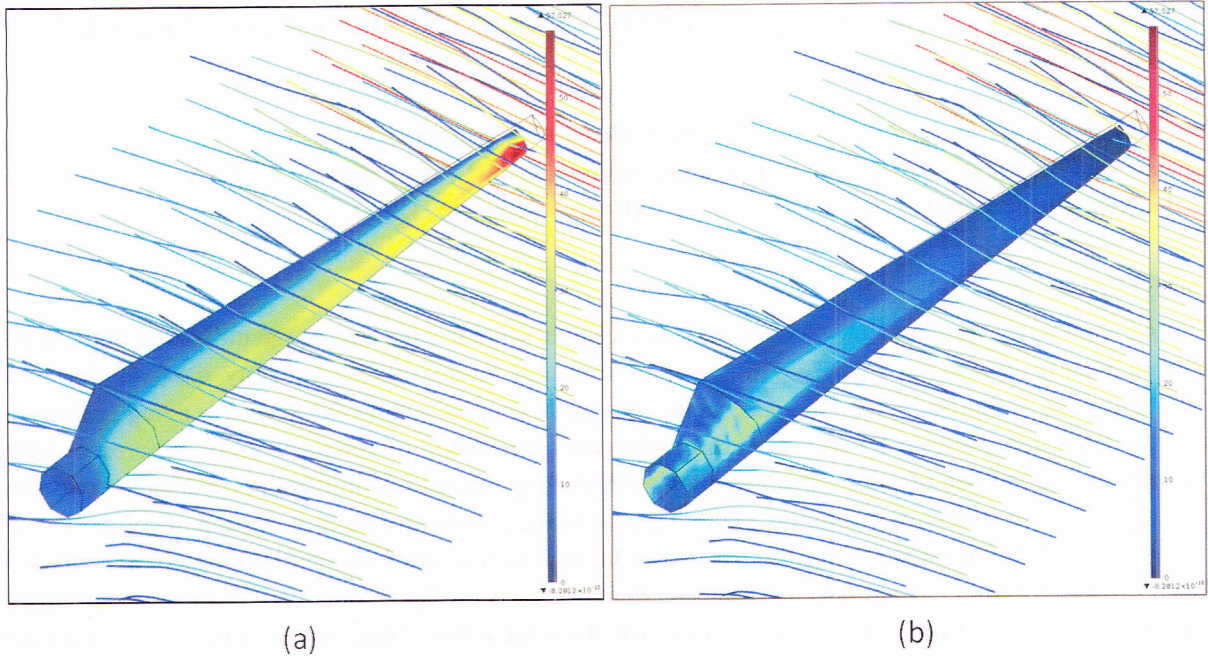


**FIG. 1:** *Fluid-Structure Interaction results with velocity stream lines superimposed. Fluid pressure distribution (a) and Von-Mises stresses distributions (b) for a typical wind turbine blade.*

tion (2b) is the equation governing the dynamics of the structure represented by the domain  $\Omega_S(t) \subset \mathbb{R}^3$ . In this equation the quantities  $\rho_S$ ,  $\tilde{\sigma}_S$ ,  $\tilde{\epsilon}_S$ ,  $u_S$  and  $b$  represent the density, the second order stress and strain tensors, and the displacement and body forces vectors respectively. The field governed by the Eq. (2c) does not have any direct physical origin but it is necessary as it provides algebraic and physical closure to the system and it describes the dynamics of the fluid mesh motion by casting it within the formalism of a fictitious or pseudo-structural subsystem. Tilded symbols denote second order tensor field state variables. The above equations are completed with their Dirichlet, Neumann or Cauchy boundary conditions as described elsewhere<sup>1-3</sup>

For the case of NACA 4-series based wind turbine blade, Fig. 1 shows a typical result produced by solving this system of equations (2) under the assumption that the material behaves elastically, for low wind velocities such as the assumptions of laminar flow can be employed.

As the ability to solve this formalism is essential for the design of wind turbine blades, the knowledge of the analytical form of the constitutive functional  $\tilde{\sigma}_S(\tilde{\epsilon}_S)$  is an essential, critical and enabling element. When this functional is linear it is known as Hooke's constitutive law. In the case where this relationship is not linear due to strain induced damage, these equations represent a more general case that allows for modeling degradation of materials.

For this reason (and in the context of aerospace naval structures), during the past decade we have embarked in an effort to automate massive multiaxial testing of composite coupons in order to determine the constitutive behavior of the bulk composite material used to make these coupons. In this paper we are reporting on an overview of a methodology and the first successful campaign of experiments for this purpose.

The approach is motivated by the data-driven requirements of employing design optimization principles for determining the constitutive behavior of composite materials as described in our recent work<sup>4,5</sup>

The constitutive characterization of composite materials has been traditionally achieved through conventional uniaxial tests and used for determining elastic properties. Typically, extraction of these properties,

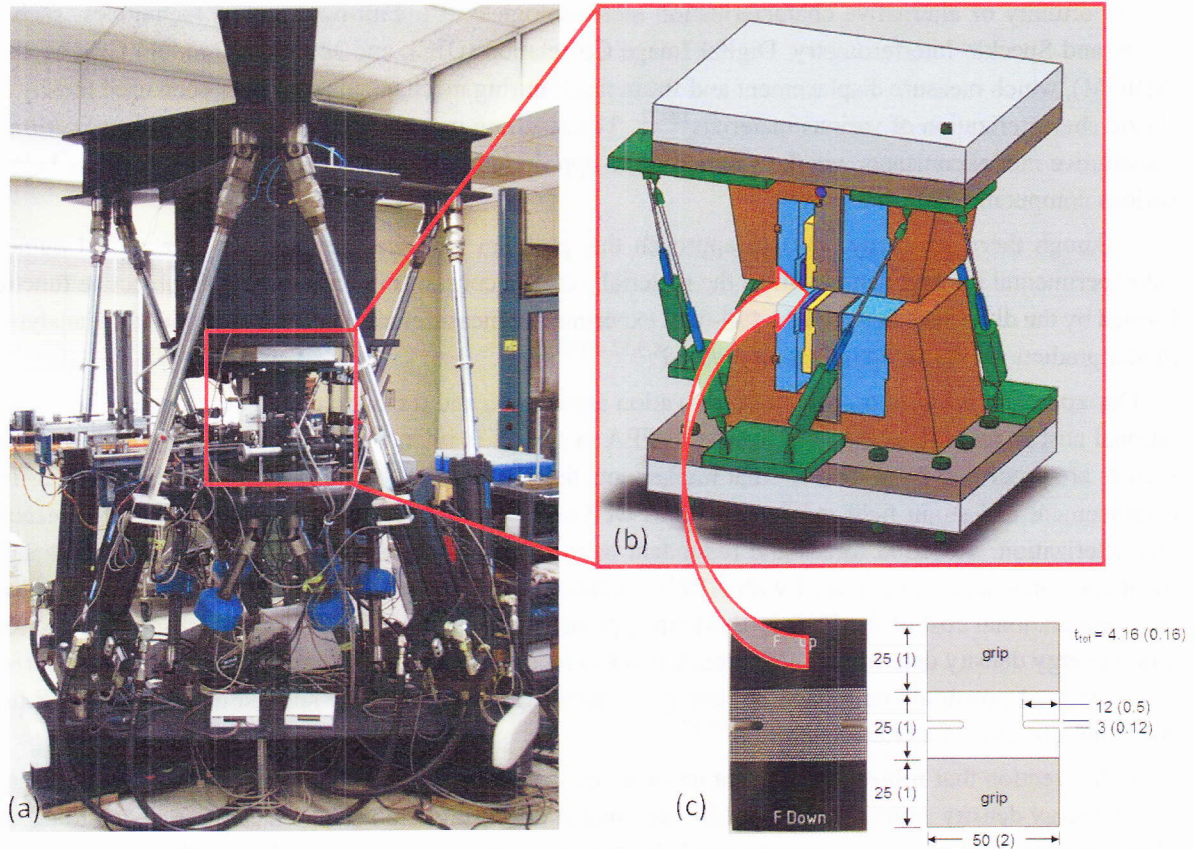


**FIG. 2:** View of the current state of NRL66.3 6-DOF mechatronically automated systems (a); view of a CAD drawing of the grip assembly (b); typical specimen view with geometrical specifications in mm (inches) (c).

involve uniaxial tests conducted with specimens mounted on uniaxial testing machines, where the major orthotropic axis of any given specimen is angled relative to the loading direction. In addition, specimens are designed such that a homogeneous state of strain is developed over a well defined area, for the purpose of measuring kinematic quantities<sup>6,7</sup>. Consequently, the use of uniaxial testing machines imposes requirements of using multiple specimens, gripping fixtures and multiple experiments. The requirement of a homogeneous state of strain frequently imposes restrictions on the sizes and shapes of specimens to be tested. Consequently, these requirements result in increased cost and time, and consequently to inefficient characterization processes.

To address these issues and to extend characterization to non-linear regimes, multi-degree of freedom automated mechatronic testing machines, which are capable of loading specimens multiaxially in conjunction with energy-based inverse characterization methodologies, were introduced at the Naval Research Laboratory (NRL)<sup>8-12</sup>. This introduction was the first of its kind and has continued through the present<sup>13-15</sup>. The most recent prototype of these machines is shown in Fig. 2.

The energy-based approach associated with mechatronic testing, although it enables multiaxial loading and inhomogeneous states of strain, still requires multiple specimens. It is significant to state however, that these specimens are tested in a automated manner with high throughput of specimens per hour, which have reached a rate of 30 specimens per hour.

The recent development of flexible full-field displacement and strain measurements methods has afforded

the opportunity of alternative characterization methodologies<sup>16–19</sup>. Full-field optical techniques, such as Moire and Speckle Interferometry, Digital Image Correlation (DIC), and Meshless Random Grid Method (MRGM), which measure displacement and strain fields during mechanical tests, have been used mostly for elastic characterization of various materials<sup>19–22</sup>. The resulting measurements are used for identification of constitutive model constants, via the solution of an appropriately formed inverse problem, with the help of various computational techniques.

Although there are many ways to approach this problem here we are focusing on a mixed numerical/experimental method that identifies the material's elastic constants by minimizing an objective function formed by the difference between the full-field experimental measurements and the corresponding analytical model predictions via an optimization method<sup>8,9,12–15,19,22–24</sup>.

Our approach is based on energy conservation arguments, and it can be classified according to computational cost in relation to the iterative use of FEA or not. It is important to clarify that digitally acquired images are processed by software<sup>25</sup> that implements the MRGM<sup>19,26–30</sup> and is used to extract the full-field displacement and strain field measurements as well as the boundary displacements required for material characterization. Reaction forces and redundant boundary displacement data are acquired from displacement and force sensors integrated with NRL's multiaxial loader called NRL66.3<sup>31</sup>. In an effort to address the computational cost of the FEA-in-the-loop approaches, the authors have initiated a dissipated and total strain energy density determination approach that has recently been extended to a framework that is derived from the total potential energy and the energy conservation, which can be applied directly with full field strain measurement for characterization<sup>32–37</sup>.

In the section that follows we present an overview of the small strain formulation (SSF) of the general strain energy density approach followed by the finite strain formulation (FSF), that are intended to capture both the linear and non-linear constitutive behavior of composite materials with or without damage. The paper continues with a description of the computational application of design optimization implementations based on these two formulations. A description of the experimental campaign and representative results follow. Finally, conclusions are presented.

## COMPOSITE MATERIAL CONSTITUTIVE RESPONSE REPRESENTATIONS

For the general case of a composite material system we consider that a modified anisotropic hyperelastic strain energy density (SED) function can be constructed to encapsulate both the elastic and the inelastic responses of the material. However, certain classes of composite materials reach failure after small strains and some under large strains. For this reason we give two example formalisms, one involving a small (infinitesimal) strain formulation (SSF) and another involving a finite (large) strain formulation (FSF).

### Small Strain Formulation

For the SSF case we have introduced a SED function that, in its most general form, can be represented as a scaled Taylor expansion of the Helmholtz free energy of a deformable body, which is expressed initially in terms of small strain invariants, and eventually of an additive decomposition in terms of a recoverable and an irrecoverable SED that can be expressed by

$$U_{SSF} = U_{SSF}^R(S; \boldsymbol{\varepsilon}_{ij}) + U_{SSF}^I(D; \boldsymbol{\varepsilon}_{ij}). \quad (3)$$

Clearly, all the second order monomials of strain components will be forming the recoverable part  $U_{SSF}^R(S; \boldsymbol{\varepsilon}_{ij})$  and the higher order monomials will be responsible for the irrecoverable part  $U_{SSF}^I(D; \boldsymbol{\varepsilon}_{ij})$ . The resulting constitutive law is given by

$$\boldsymbol{\sigma}_{ij} = \partial U_{SSF} / \partial \boldsymbol{\varepsilon}_{ij} = \partial (U_{SSF}^R(S; \boldsymbol{\varepsilon}_{ij}) + U_{SSF}^I(D; \boldsymbol{\varepsilon}_{ij})) / \partial \boldsymbol{\varepsilon}_{ij} \quad (4)$$

A general expression which provides the strain dependent version of Eq. 3 after the expansion of the strain

invariants<sup>4</sup>, is given by

$$U_{SSF} = U_{SSF}^R(S; \boldsymbol{\varepsilon}_{ij}) + U_{SSF}^I(D; \boldsymbol{\varepsilon}_{ij}) = \frac{1}{2} s_{ijkl} \boldsymbol{\varepsilon}_{ij} \boldsymbol{\varepsilon}_{kl} + d_{ijkl}(\boldsymbol{\varepsilon}_{ij}) \boldsymbol{\varepsilon}_{ij} \boldsymbol{\varepsilon}_{kl} \quad (5)$$

where  $s_{ijkl}$  are the components of the elastic stiffness tensor (Hooke's tensor) and  $d_{ijkl}(\boldsymbol{\varepsilon}_{ij})$  are strain-dependent damage functions, which fully define irrecoverable (or dissipated) strain energy density given by enforcing the dissipative nature of energy density. The quantity  $d_{ijkl}(\boldsymbol{\varepsilon}_{ij})$  can be defined in a manner analogous to that employed for the 1D system described elsewhere<sup>4</sup> and is given by

$$d_{ijkl}(\boldsymbol{\varepsilon}_{ij}) = s_{ijkl} \left( 1 - e^{-\frac{\boldsymbol{\varepsilon}_{ij}^{p_{ij}}}{q_{ij}} / (ep_{ij})} \right) \quad (6)$$

A follow-up series expansion and subsequent drop of all terms except the first is enough in capturing almost all of the characteristics of dissipative behavior, yielding,

$$d_{ijkl}(\boldsymbol{\varepsilon}_{ij}) = s_{ijkl} \sum_{m=1}^n (-1)^m \left( \frac{1}{ep_{ij}} \right)^m \frac{\boldsymbol{\varepsilon}_{ij}^{mp_{ij}}}{m! q_{ij}^{mp_{ij}}} \simeq -s_{ijkl} \left( \frac{1}{ep_{ij}} \right) \frac{\boldsymbol{\varepsilon}_{ij}^{p_{ij}}}{q_{ij}^{p_{ij}}} \quad (7)$$

Thus the irrecoverable part of the energy in Eq. 3 becomes

$$U_{SSF}^I(D; \boldsymbol{\varepsilon}_{ij}) = U_{SSF}^I(s_{ijkl}, p_{ij}, q_{ij}; \boldsymbol{\varepsilon}_{ij}) = -s_{ijkl} \frac{1}{e(2+p_{ij}) p_{ij} q_{ij}^{p_{ij}}} \boldsymbol{\varepsilon}_{ij}^{1+p_{ij}} \boldsymbol{\varepsilon}_{kl} \quad (8)$$

Next, substituting Eq. 6 into Eq. 3 yields

$$\begin{aligned} U_{SSF} &= U_{SSF}^R(S; \boldsymbol{\varepsilon}_{ij}) + U_{SSF}^I(D; \boldsymbol{\varepsilon}_{ij}) = \\ &= \frac{1}{2} s_{ijkl} \boldsymbol{\varepsilon}_{ij} \boldsymbol{\varepsilon}_{kl} - s_{ijkl} \frac{1}{e(2+p_{ij}) p_{ij} q_{ij}^{p_{ij}}} \boldsymbol{\varepsilon}_{ij}^{1+p_{ij}} \boldsymbol{\varepsilon}_{kl} \end{aligned} \quad (9)$$

Applying Eq. 4 on Eq. 7, and employing Voigt<sup>6</sup> notation for the case of a general orthotropic material, yields the constitutive relation

$$\begin{bmatrix} \sigma_{xx} \\ \sigma_{yy} \\ \sigma_{zz} \\ \sigma_{xz} \\ \sigma_{yz} \\ \sigma_{xy} \end{bmatrix} = \begin{bmatrix} \check{s}_{xx} & s_{xy} & s_{xz} & 0 & 0 & 0 \\ s_{xy} & \check{s}_{yy} & s_{yz} & 0 & 0 & 0 \\ s_{xz} & s_{yz} & \check{s}_{zz} & 0 & 0 & 0 \\ 0 & 0 & 0 & \check{s}_{xz} & 0 & 0 \\ 0 & 0 & 0 & 0 & \check{s}_{yz} & 0 \\ 0 & 0 & 0 & 0 & 0 & \check{s}_{xy} \end{bmatrix} \begin{bmatrix} \boldsymbol{\varepsilon}_{xx} \\ \boldsymbol{\varepsilon}_{yy} \\ \boldsymbol{\varepsilon}_{zz} \\ \boldsymbol{\varepsilon}_{xz} \\ \boldsymbol{\varepsilon}_{yz} \\ \boldsymbol{\varepsilon}_{xy} \end{bmatrix} \quad (10)$$

where:

$$\check{s}_{ij} = s_{ij} (1 - \bar{d}_{ij}) \quad (11)$$

and

$$\bar{d}_{ij} = \frac{1}{ep_{ij} q_{ij}^{p_{ij}}} \boldsymbol{\varepsilon}_{ij}^{1+p_{ij}} \quad (12)$$

The orthotropic symmetry requirements involve material parameters that are the 9 elastic  $s_{ij}$  constants and  $6 \times 2 = 12$  damage constants  $p_{ij}$ ,  $q_{ij}$  for a total of 21 parameters. Clearly, when the quantities  $\bar{d}_{ij}$  do not depend on the strains and they are constants, Eq. 8 reduces to most of the continuous damage theories given by various investigators in the past<sup>38-41</sup>. For a transversely isotropic material the number of material parameters drops to  $5+10=15$  for a 3D state of strain and to  $4+8=12$  for a plane stress state.

#### Finite Strain Formulation

The FSF can be written in a double additive decomposition manner. The first being the decomposition of the recoverable and irrecoverable SED, and the second being the decomposition between the volumetric

(or dilatational)  $W_v$  and the distortional (or isochoric)  $W_d$  parts of the total SED. This decomposition is expressed by:

$$\begin{aligned} U_{SSF} &= U_{SSF}^R(\alpha_i; J, \bar{C}) + U_{SSF}^I(\alpha_i, \beta_i; J, \bar{C}) = \\ &= [W_v(J) + W_d(\bar{C}, A \otimes A, B \otimes B)] - [d_v W_v(J) + d_d W_d(\bar{C}, A \otimes A, B \otimes B)] \end{aligned} \quad (13)$$

where  $\alpha_i, \beta_i$  are the elastic and inelastic material parameters of the system, respectively. A rearrangement of these decompositions, such as the volumetric vs. distortional decomposition, which appears on the highest expression level, leads to an expression introduced in<sup>42</sup>, i.e.,

$$U_{SSF} = (1 - d_v)W_v(J) + (1 - d_d)W_d(\bar{C}, A \otimes A, B \otimes B), \quad (14)$$

with the damage parameters  $d_k \in [0, 1], k \in [v, d]$  defined as

$$d_k = d_{ka}^\infty \left[ 1 - e^{-\frac{a_k(t)}{\eta_{ka}}} \right] \quad (15)$$

where  $a_k(t) = \max_{s \in [0, t]} W_k^o(s)$  is the maximum energy component reached so far, and  $d_{ka}^\infty, \eta_{ka}$  are two pairs of parameters controlling the energy dissipation characteristics of the two components of SED. In this formulation,  $J = \det \underline{F}$  is the Deformation Gradient,  $\bar{C} = \underline{F}^T \underline{F}$  is the right Cauchy Green (Green deformation) tensor,  $A, B$  are constitutive material directions in the undeformed configuration, and  $A \otimes A, B \otimes B$  are microstructure structural tensors expressing fiber directions. Each of the two components of SED are defined as

$$\begin{aligned} W_v(J) &= \frac{1}{d}(J-1)^2 W_d(\bar{C}, A \otimes A, B \otimes B) = \\ &= \sum_{i=1}^3 a_i (\bar{I}_1 - 3)^i + \sum_{j=1}^3 b_j (\bar{I}_2 - 3)^j + \sum_{k=1}^6 c_k (\bar{I}_4 - 1)^k + \\ &+ \sum_{l=2}^6 d_l (\bar{I}_5 - 1)^l + \sum_{m=2}^6 e_m (\bar{I}_6 - 1)^m + \sum_{n=2}^6 f_n (\bar{I}_7 - 1)^n + \sum_{o=2}^6 g_o (\bar{I}_8 - (A \cdot B)^2)^o \end{aligned} \quad (16)$$

where the strain invariants are defined as follows:

$$\begin{aligned} \bar{I}_1 &= \text{tr} \bar{C}, \quad \bar{I}_2 = \frac{1}{2}(\text{tr}^2 \bar{C} - \text{tr} \bar{C}^2) \\ \bar{I}_4 &= A \cdot \bar{C} B, \quad \bar{I}_5 = A \cdot \bar{C}^2 B \\ \bar{I}_6 &= B \cdot \bar{C} B, \quad \bar{I}_7 = B \cdot \bar{C}^2 B, \quad \bar{I}_8 = (A \cdot B) A \cdot \bar{C} B \end{aligned} \quad (17)$$

The corresponding constitutive behavior is given by the second Piola-Kirchhoff stress tensor according to<sup>39</sup>

$$S = 2 \frac{\partial U_{SSF}}{\partial C} \quad (18)$$

or the usual Cauchy stress tensor according to

$$\sigma_{FSF} = \frac{2}{J} F \cdot \frac{\partial U_{SSF}}{\partial C} \cdot F^T. \quad (19)$$

Under the FSF formulation the material characterization problem involves determining the 36 coefficients (at most) of all monomials when the sums in the expression of distortional SED are expanded in Eq. 16, in addition to the compressibility constant  $d$  and the 4 parameters used in Eq. 15. It follows that potentially there can be a total of 41 material constants.

## COMPUTATIONAL IMPLEMENTATION

In order to determine the material parameters the inverse problem at hand is solved through a design optimization approach that is described by the logic depicted in Fig. 3. The implementation of this logic involved a computational infrastructure that controlled by Matlab, where the forward solution of the in-

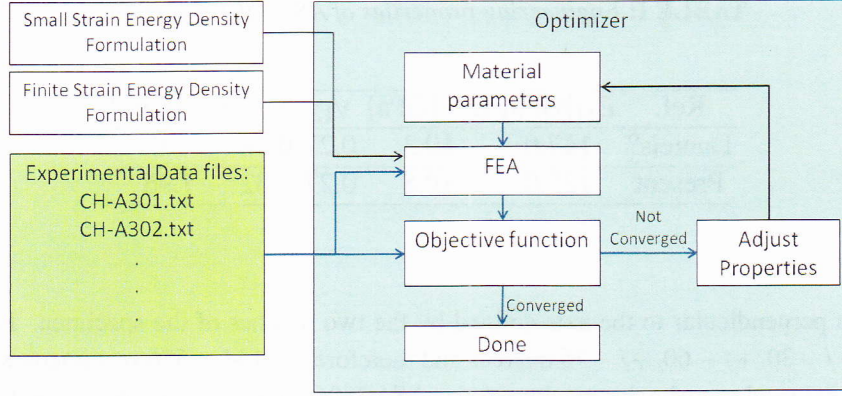


**FIG. 3:** Overview of design optimization logic.

stantaneous FEA was accomplished by ANSYS. Due to the costly calculations we created a virtual cluster that essentially used the multiple cores available in three systems, via a spawning 102 virtual machines capable of running 102 instances of ANSYS in a parallel fashion, whereas each process was responsible for a different subdomain of the design space as described in<sup>43</sup>.

Details of the FEM model used for the specimens constructed and tested are not presented here due to the space limitations but they can be found in<sup>4,5</sup>.

Two objective functions were constructed. Both utilized the fact that through the REMDIS-3D software<sup>44</sup>, developed by our group, one can obtain full field measurements of the displacement and strain fields over any deformable body as an extension of the REMDIS-2D software that is based on the MRGM<sup>19,25–30</sup>. Thus, our experimental measurements for the formation of the objective functions were chosen to be the strains at the nodal points of the FEM discretization. The first objective function chosen was based entirely on strains and is given by

$$J^e = \sum_{k=1}^N \left( \sum_{i=1}^2 \sum_{j=i}^2 \left( \left[ \boldsymbol{\varepsilon}_{ij}^{\text{exp}} \right]_k - \left[ \boldsymbol{\varepsilon}_{ij}^{\text{fem}} \right]_k \right) \right)^2, \quad (20)$$

the second objective function is given in terms of surface strain energy density according to

$$\begin{aligned} J^U &\approx \oint_{\partial\Omega} (U^{\text{exp}} - U^{\text{fem}})^2 dS \approx \\ &\approx \oint_{\partial\Omega} \left( \sum_{i=1}^2 \sum_{j=i}^2 \sum_{m=1}^2 \sum_{n=m}^2 \left( s_{ijmn} \boldsymbol{\varepsilon}_{ij}^{\text{exp}} \boldsymbol{\varepsilon}_{mn}^{\text{exp}} - s_{ijmn} \boldsymbol{\varepsilon}_{ij}^{\text{fem}} \boldsymbol{\varepsilon}_{mn}^{\text{fem}} \right) \right)^2 dS \end{aligned} \quad (21)$$

where  $\left[ \boldsymbol{\varepsilon}_{ij}^{\text{exp}} \right]_k$ ,  $\left[ \boldsymbol{\varepsilon}_{ij}^{\text{fem}} \right]_k$  are the experimentally determined and the FEM produced components of strain are at node  $k$ . The quantities  $U^{\text{exp}}, U^{\text{fem}}$  are the surface strain energy densities formulated by using the experimental strains and the FEM produced strains respectively.

Both objective functions were implemented, and we utilized both the DIRECT global optimizer<sup>45</sup>, which is available for Matlab<sup>46</sup>, and a custom developed Monte-Carlo optimizer, also implemented in Matlab.

## EXPERIMENTAL CAMPAIGN

Based on an analysis that falls outside the scope of the present paper<sup>47</sup>, we identified 72 proportional loading paths to sample the 6-DoF space defined by the 3 translations and 3 rotations that can be applied by the moveable grip of the NRL66.3. We selected to use a single specimen per loading path and then repeat the process. That requires 144 specimens per material system. Each material system was defined to be a balanced laminate with an alternating angle of fiber inclination per ply relative to the vertical axis of the

**TABLE I:** Engineering properties of AS4/3501-6 laminae

Ref.	$E_{11}$ [GPa]	$E_{22}$ [GPa]	$\nu_{12}$	$\nu_{23}$	$G_{12}$ [GPa]
Daniels <sup>6</sup>	147.0	10.3	0.27	0.28	7.0
Present	125.0	10.8	0.27	0.32	7.96

specimen that is perpendicular to the axis defined by the two notches of the specimen. Four angles were used  $+/- 15, +/- 30, +/- 60, +/- 75$  degrees and therefore  $4 \times 144 = 576$  specimens were constructed. The actual material used to make the specimens was AS4/3506-1 epoxy resin/fiber respectively.

All specimens were tested by using NRL66.3 in May of 2011. In May 13, 2011, the system achieved a throughput of 20 test/hour for a total of 132 tests. On May 27 the system achieved a throughput of 25 tests/hour for a total of 216 tests. On June 15, 2011 the system reached its peak throughput of 28 tests/hour. All 1152 tests were completed in 12 work-days. The test yielded 13 TB of data from the sensors and the cameras of the system. Typical experimental data are shown in a more detailed reference<sup>43</sup>.

Using the collected data and the optimization approach outlined earlier for the case of the SSF we identified the elastic constants as shown in Table 1, in comparison to those of<sup>6</sup>. By running FEA for the cases that correspond to the specific loading path corresponding to an experiment we can now compare the predicted distribution of any component of the strain or stress tensor. In order to demonstrate how well the FSF formulation can capture the behavior of the characterization coupons used to obtain the data utilized in the characterization process we are presenting typical examples in terms of the distributions of  $\epsilon_{yy}$  as measured by the MRGM (left column) and as predicted by the FSF theory (right column), for both the front (top row) and the back (bottom row) of Figs. 4, 5.

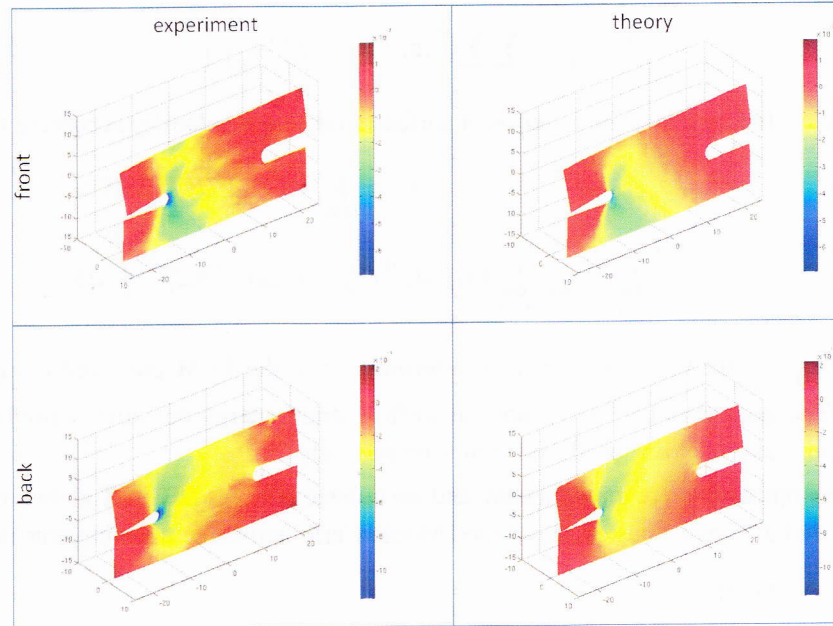


**FIG. 4:** Comparison of  $(\epsilon_{yy})$  field between measured (left) and the identified model by using the FSF for the case of in plane rotation and torsion of a  $+/- 30$  degrees laminate

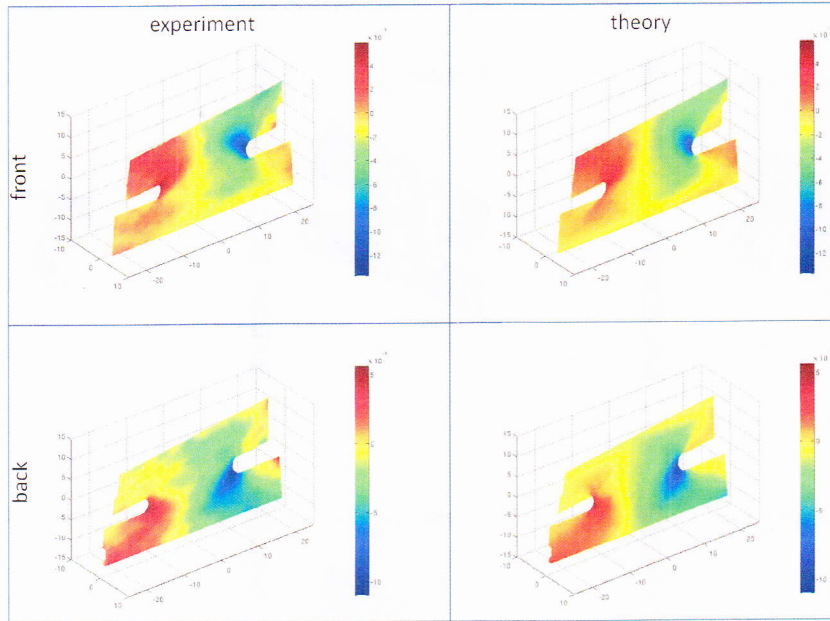


**FIG. 5:** Comparison of  $(\epsilon_{yy})$  field between measured (left) and the identified model by using the FSF for the case of in-plane rotation and torsion of a +/- 60 degrees laminate

## VALIDATION

The characterization methodology described here and in our previous publications, utilized the data described herein along with the data from other validation tests performed on structures of different shape and layups than that of the characterization coupons, to perform validation comparisons. A discussion of this activity is presented elsewhere<sup>48</sup> in more detail.

Here we present validation based on the typical double notched characterization specimen described in<sup>43</sup>, but for loading paths that were not used for determining the constitutive model itself.

As a representative validation prediction we are presenting the results for two loading paths. It is important to emphasize that the experimental data obtained from the associated tests were not used in determining the constitutive constants (material parameters) that are fixing the associated constitutive model.

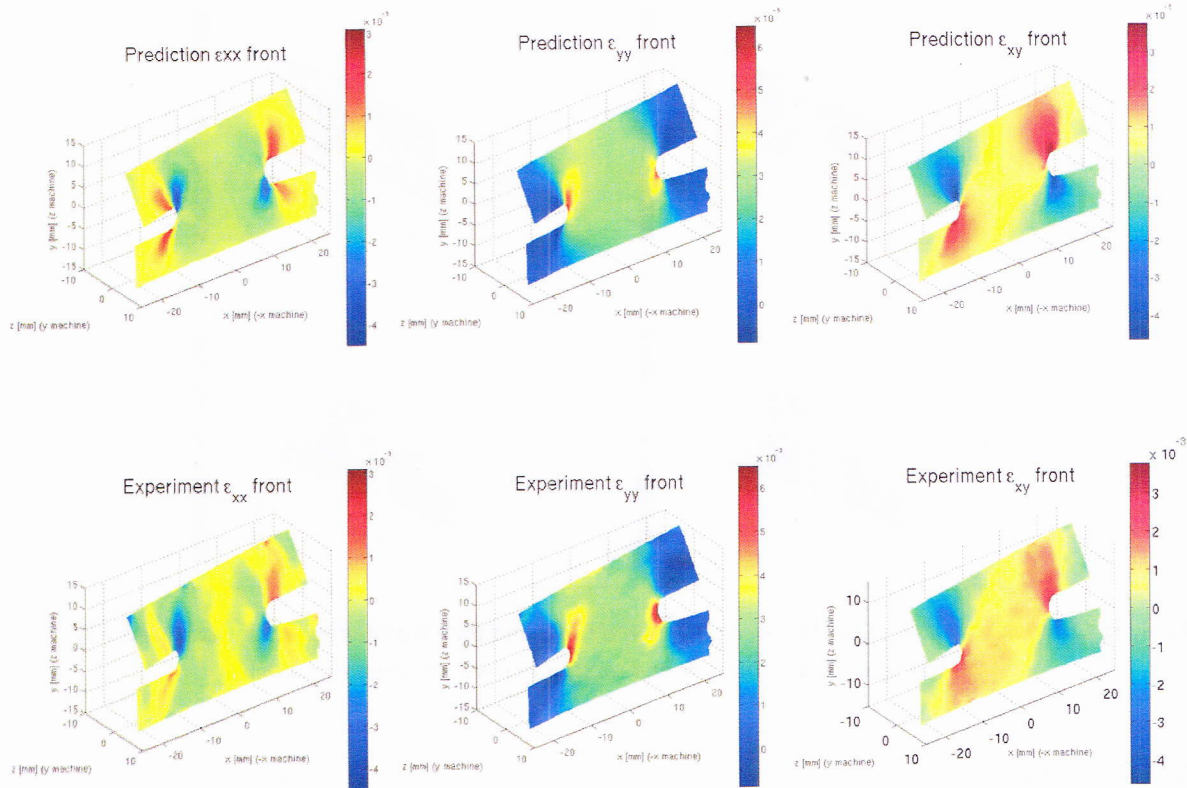
Figure 6 shows the three strain field distributions at the same loading step of a load path that involves tension, bending and torsion about the vertical axis.

Figure 7 shows the three strain field distributions at the same loading step of a load path that involves in plane rotation and torsion. All predicted strain field distributions for both of these cases, show that the predicted values are within 4% error of the experimental ones. This is within the error of the RemDiS-3D experimental method for that level of strain, except very few areas of high strain gradients.

## CONCLUSIONS AND PLANS

We have described and outline of a multiaxial automated composite material characterization methodology that utilizes multiaxial experiments performed with the NRL66.3 mechatronic system.

Design optimization methodologies for the determination of the constitutive response of composite materials with or without damage has been employed. Strain energy density and full field strain based approaches have been utilized to incorporate massive full field strain measurements from specimens loaded by a custom-made multiaxial loading machine. We have formulated objective functions expressing the difference between the experimentally observed behavior of composite materials under various loading condi-



**FIG. 6:** Predicted (top row) vs. experimental (bottom row) strain component fields distributions for a characterization coupon under combined tension, bending and torsion loading

tions, and the simulated behavior via FEA, which are formulated in terms of strain energy density functions of a particular structure under identical loading conditions.

Two formalisms involving small strains and finite strains have been utilized in a manner that involves both additive decomposition of recoverable and irrecoverable strain energy density. This was done in order to address both the elastic and inelastic response of composite materials due to damage. The finite strain formulation further involves a volumetric and distortional energy decomposition.

Representative results of the characterization have been compared with the associated experimental ones to demonstrate how well they agree.

Finally, for the validation purposes, we have presented a comparison of behavior predictions from FEA models based on the characterized constitutive behavior for the SSF vs. experimental results of characterization coupons not used for the characterization.

The coincidence between experiment and prediction for all tests conducted, clearly suggests our characterization methodology is successful in identifying the proper constitutive behavior and the associated material parameters.

This success provides confidence into pursuing our plans for utilizing the energy-based constitutive characterization to formulate failure criteria and address the very important issue of predicting failure for design and maintainability purposes of wind turbine blade applications.

#### ACKNOWLEDGEMENT

The authors acknowledge support for this work by the Office of Naval Research and the Naval Research

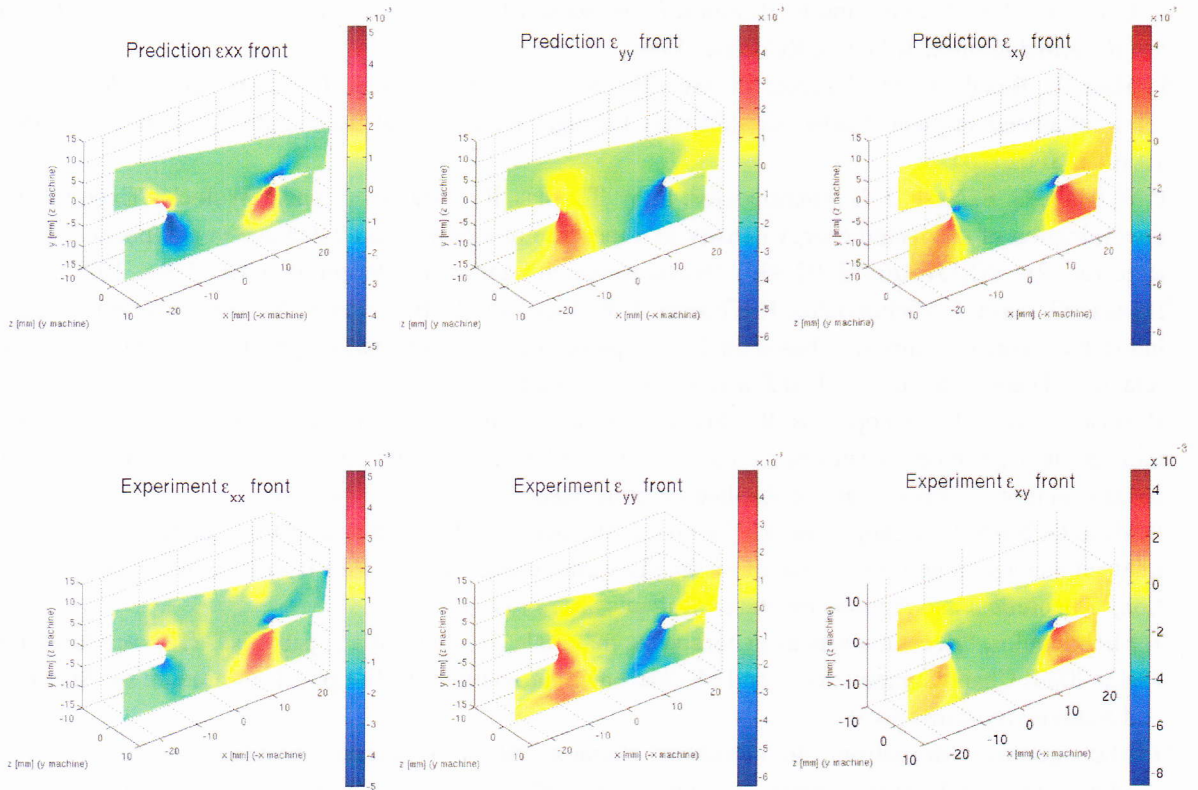


**FIG. 7:** Predicted (top row) vs. experimental (bottom row) strain component fields distributions for a characterization coupon under combined in-plane rotation and torsion loading

Laboratory's core funding.

## REFERENCES

- <sup>1</sup>J. Michopoulos, C. Farhat, and J. Fish, "Modeling and simulation of multiphysics systems," *Journal of Computing and Information Science in Engineering* **5**, 198–213 (2005).
- <sup>2</sup>M. Lesoinne and C. Farhat, in *11th AIAA Computational Fluid Dynamics Conference* (AIAA, Orlando, Florida, 1993) pp. AIAA Paper No. 93–3325 1993.
- <sup>3</sup>P. Geuzaine, G. Brown, and C. Farhat, "Three-field based nonlinear aeroelastic simulation technology: Status and application to the flutter analysis of an f-16 configuration," in *40th Aerospace Sciences Meeting and Exhibit*, AIAA Paper 2002-0870 (Reno, Nevada, USA, 2002) pp. 14–17.
- <sup>4</sup>J. Michopoulos, J. Hermanson, A. Iliopoulos, S. Lambrakos, and T. Furukawa, "Data-driven design optimization for composite material characterization," *Journal of Computing and Information Science in Engineering* **11** (2011).
- <sup>5</sup>J. Michopoulos, J. C. Hermanson, A. Iliopoulos, S. Lambrakos, and T. Furukawa, "Overview of constitutive response characterization for composite materials via data-driven design optimization," in *Proceedings of the ASME 2011 International Design Engineering Technical Conferences & Computers and Information in Engineering Conference IDETC/CIE, August 29-31, 2011, Washington, DC, USA* (2011).
- <sup>6</sup>I. M. Daniel and O. Ishai, *Engineering Mechanics of Composite Materials*, 2nd ed. (Oxford University

- Press, USA, 2005).
- <sup>7</sup>L. Carlsson, D. F. Adams, and R. B. Pipes, *Experimental Characterization of Advanced Composite Materials, Third Edition*, 3rd ed. (CRC Press, 1986).
  - <sup>8</sup>P. Mast, L. Beaubien, M. Clifford, D. Mulville, S. Sutton, R. Thomas, J. Tirosh, and I. Wolock, "A semi-automated in-plane loader for materials testing," *Experimental Mechanics* **23**, 236–241 (1983), 10.1007/BF02320415.
  - <sup>9</sup>P. W. Mast, G. E. Nash, J. G. Michopoulos, R. W. Thomas, R. Badaliane, and I. Wolock, "Experimental determination of dissipated energy density as a measure of strain-induced damage in composites," Tech. Rep. Tec. Rpt. NRL/FR/6383–92–9369 (Naval Research Laboratory, Washington, DC, USA, 1992).
  - <sup>10</sup>P. Mast, G. Nash, J. Michopoulos, R. Thomas, I. Wolock, and R. Badaliane, "Characterization of strain-induced damage in composites based on the dissipated energy density part iii. general material constitutive relation," *Theoretical and Applied Fracture Mechanics* **22**, 115–125 (1995).
  - <sup>11</sup>P. Mast, G. Nash, J. Michopoulos, R. Thomas, I. Wolock, and R. Badaliane, "Characterization of strain-induced damage in composites based on the dissipated energy density part II. Composite specimens and naval structures," *Theoretical and Applied Fracture Mechanics* **22**, 97–114 (1995).
  - <sup>12</sup>P. Mast, G. Nash, J. Michopoulos, R. Thomas, I. Wolock, and R. Badaliane, "Characterization of strain-induced damage in composites based on the dissipated energy density Part I. Basic scheme and formulation," *Theoretical and Applied Fracture Mechanics* **22**, 71–96 (1995).
  - <sup>13</sup>J. Michopoulos, "Recent advances in composite materials: In honor of s.a. paipetis," (Kluwer Academic Press, 2003) Chap. Computational and Mechatronic Automation of Multiphysics Research for Structural and Material Systems, pp. 9–21.
  - <sup>14</sup>J. Michopoulos, "Mechatronically automated characterization of material constitutive response," in *Proceedings of the 6th World Congress on Computational Mechanics (WCCM-VI)* (Tsinghua University Press and Springer, Beijing China, 2004) pp. 486–491.
  - <sup>15</sup>J. Michopoulos, J. Hermanson, and T. Furukawa, "Towards the robotic characterization of the constitutive response of composite materials," *Composite Structures* **86**, 154–164 (2008).
  - <sup>16</sup>F. Pierron, G. Vert, R. Burguete, S. Avril, R. Rotinat, and M. R. Wisnom, "Identification of the orthotropic elastic stiffnesses of composites with the virtual fields method: Sensitivity study and experimental validation," *Strain* **43**, 250–259 (2007).
  - <sup>17</sup>S. Cooreman, D. Lecompte, H. Sol, J. Vantomme, and D. Debruyne, "Elasto-plastic material parameter identification by inverse methods: Calculation of the sensitivity matrix," *International Journal of Solids and Structures* **44**, 4329 – 4341 (2007).
  - <sup>18</sup>T. Furukawa and J. Michopoulos, "Computational design of multiaxial tests for anisotropic material characterization," *International Journal for Numerical Methods in Engineering* **74**, 1872–1895 (2008).
  - <sup>19</sup>J. G. Michopoulos, A. P. Iliopoulos, and T. Furukawa, "Accuracy of inverse composite laminate characterization via the mesh free random grid method," *ASME Conference Proceedings* **2009**, 367–374 (2009).
  - <sup>20</sup>L. Bruno, F. M. Furgiuele, L. Pagnotta, and A. Poggialini, "A full-field approach for the elastic characterization of anisotropic materials," *Optics and Lasers in Engineering* **37**, 417 – 431 (2002).
  - <sup>21</sup>T. Schmidt, J. Tyson, and K. Galanulis, "Full-field dynamic displacement and strain measurement using advanced 3d image correlation photogrammetry: Part 1," *Experimental Techniques* **27**, 47–50 (2003).
  - <sup>22</sup>J. Kajberg and G. Lindkvist, "Characterisation of materials subjected to large strains by inverse modelling based on in-plane displacement fields," *International Journal of Solids and Structures* **41**, 3439 – 3459 (2004).
  - <sup>23</sup>M. H. H. Meuwissen, C. W. J. Oomens, F. P. T. Baaijens, R. Petterson, and J. D. Janssen, "Determination of the elasto-plastic properties of aluminium using a mixed numerical-experimental method," *Journal of Materials Processing Technology* **75**, 204 – 211 (1998).
  - <sup>24</sup>J. Molimard, R. Le Riche, A. Vautrin, and J. Lee, "Identification of the four orthotropic plate stiffnesses

- using a single open-hole tensile test,” *Experimental Mechanics* **45**, 404–411 (2005), 10.1007/BF02427987.
- <sup>25</sup>J. G. Michopoulos and A. P. Iliopoulos, “A computational workbench for remote full field 2d displacement and strain measurements,” *ASME Conference Proceedings* **2009**, 55–63 (2009).
- <sup>26</sup>N. P. Andrianopoulos and A. P. Iliopoulos, “Displacements measurement in irregularly bounded plates using mesh free methods,” in *Proc. 16th European Conference of Fracture, Alexandroupolis, Greece, July 3–7* (2006).
- <sup>27</sup>A. P. Iliopoulos, J. G. Michopoulos, and N. P. Andrianopoulos, “Performance sensitivity analysis of the Mesh-Free Random Grid method for whole field strain measurements,” *ASME Conference Proceedings* **2008**, 545–555 (2008).
- <sup>28</sup>A. P. Iliopoulos, J. G. Michopoulos, and N. P. Andrianopoulos, “Performance analysis of the Mesh-Free Random Grid Method for full-field synthetic strain measurements,” *Strain*, In Print (2010).
- <sup>29</sup>A. Iliopoulos and J. Michopoulos, “Sensitivity analysis of the mesh-free random grid method for measuring deformation fields on composites,” in *Proceedings of the 17th International Conference on Composite Materials, ICCM-17, Edinburgh* (The British Composites Society: Edinburgh International Convention Centre (EICC), Edinburgh, UK, 2009, 27–31 Jul 2009).
- <sup>30</sup>A. P. Iliopoulos and J. G. Michopoulos, “Effects of anisotropy on the performance sensitivity of the Mesh-Free random grid method for whole field strain measurement,” *ASME Conference Proceedings* **2009**, 65–74 (2009).
- <sup>31</sup>J. G. Michopoulos, J. C. Hermanson, and A. Iliopoulos, “Towards a recursive hexapod for the multidimensional mechanical testing of composites,” in *Proceedings of the ASME 2010 International Design Engineering Technical Conferences & Computers and Information in Engineering Conference IDETC/CIE 2010*, DETC2010/CIE-28699 (2010).
- <sup>32</sup>J. Michopoulos and T. Furukawa, “Multi-level coupling of dynamic data-driven experimentation with material identification,” *Lecture Notes in Computer Science (including subseries Lecture Notes in Artificial Intelligence and Lecture Notes in Bioinformatics)* **4487 LNCS**, 1180–1188 (2007).
- <sup>33</sup>T. Furukawa, J. Michopoulos, and D. Kelly, “Elastic characterization of laminated composites based on multi-axial tests,” *Composite Structures* **86**, 269–278 (2008).
- <sup>34</sup>H. Man, T. Furukawa, and D. Kellermann, “Implicit constitutive modeling based on the energy principles,” in *Proceedings of XXII ICTAM, 25-29 August 2008, Adelaide 2008* (2008).
- <sup>35</sup>T. Furukawa and J. Michopoulos, “Online planning of multi-axial loading paths for elastic material identification,” *Computer Methods in Applied Mechanics and Engineering* **197**, 885–901 (2008).
- <sup>36</sup>J. Michopoulos, T. Furukawa, and S. Lambrakos, “Data-driven characterization of composites based on virtual deterministic and noisy multi-axial data,” in *2008 ASME International Design Engineering Technical Conferences and Computers and Information in Engineering Conference, DETC 2008*, Vol. 3 (New York City, NY, 2009) pp. 1095–1106.
- <sup>37</sup>T. Furukawa and J. W. Pan, “Stochastic identification of elastic constants for anisotropic materials,” *International Journal for Numerical Methods in Engineering* **81**, 429–452 (2010).
- <sup>38</sup>R. Haj-Ali and H.-K. Kim, “Nonlinear constitutive models for FRP composites using artificial neural networks,” *Mechanics of Materials* **39**, 1035 – 1042 (2007).
- <sup>39</sup>P. Haupt, *Continuum Mechanics and Theory of Materials*, 2nd ed. (Springer, 2002).
- <sup>40</sup>F. Van Der Meer and L. Sluys, “Continuum models for the analysis of progressive failure in composite laminates,” *Journal of Composite Materials* **43**, 2131–2156 (2009), <http://jcm.sagepub.com/content/43/20/2131.full.pdf+html>.
- <sup>41</sup>J. W. Ju, J. Chaboche, and G. Z. Voyiadjis, *Damage Mechanics in Engineering Materials*, 1st ed. (Elsevier Science, 1998).
- <sup>42</sup>M. Kaliske, “A formulation of elasticity and viscoelasticity for fibre reinforced material at small and finite strains,” *Comput. Meth. Appl. Mech. Eng.* **185**, 225–243 (2000).

- <sup>43</sup>J. Michopoulos, J. C. Hermanson, and A. Iliopoulos, "First industrial strength multi-axial robotic testing campaign for composite material characterization," in *Proceedings of the ASME 2012 International Design Engineering Technical Conferences & Computers and Information in Engineering Conference IDETC/CIE, August 12-15, 2012, Chicago, IL, USA* (2012) submitted.
- <sup>44</sup>J. Michopoulos and A. Iliopoulos, "A computational workbench for remote full field 3d displacement and strain measurements," in *Proceedings of the ASME 2011 International Design Engineering Technical Conferences & Computers and Information in Engineering Conference IDETC/CIE, August 29-31, 2011, Washington, DC, USA* (2011).
- <sup>45</sup>D. R. Jones, C. D. Perttunen, and B. E. Stuckman, "Lipschitzian optimization without the Lipschitz constant," *J. Optim. Theory Appl.* **79**, 157–181 (1993).
- <sup>46</sup>The Mathworks, "Matlab," <http://www.mathworks.com>.
- <sup>47</sup>A. P. Iliopoulos and J. G. Michopoulos, "Loading subspace selection for multidimensional characterization tests via computational experiments," *ASME Conference Proceedings* **2010**, 101–110 (2010).
- <sup>48</sup>J. Michopoulos, H. J. C., and A. Iliopoulos, "Robotic and multiaxial testing for the constitutive characterization of composites," in *Materials Challenges in Alternative & Renewable Energy, February 26-March 1, 2012, Clearwater, FL, USA* (2012).